An Improved Image-Based Near-Field-to-Far-Field Transformation for Cylindrical Scanning Surfaces

Hirokazu Kobayashi[1], Andrey Osipov[2], and Hirosuke Suzuki[3]

[1]Department of Information Engineering, Niigata University, 2-8050 Ikarashi, Nishi-ku, Niigata 950-2181, Japan, kobayashi@ie.niigata-u.ac.jp

[2]Microwave and Radar Institute, German Aerospace Center (DLR), Muenchner Str. 20, Wessling 82234, Germany, andrey.osipov@dlr.de

[3]KEYCOM Corporation, 3-40-2 Minamiotsuka, Toshima-ku, Tokyo 170-0005, Japan, suzuki@keycom.co.jp

Abstract

An improved image-based circular near-field-to-far-field transformation (NFFFT) developed recently by the authors for smaller measurement facilities and for targets with pronounced scattering centers offset from the center of the imaging area is extended to a cylindrical scanning surface. Scanning over a surface instead of a circle permits RCS estimations for targets whose size in the direction perpendicular to the measurement plane is comparable to their extension in the measurement plane. The approach consists in near-field imaging of the target, followed by integration of the image. The focusing operator, which is used to generate the image, is built in such a way so that the image of an electrically small PEC sphere is exactly the delta function. The paper describes the effect of various transformation parameters such the sampling rates in the input data and in the image domain on the quality of RCS estimations.

1. Introduction

Direct measurements of RCS of electrically large objects are hardly possible because of the too distant location of the far-field region, in which RCS is defined. The location of the far zone is determined by the relation $2D^2/\lambda$ where D is the characteristic size of the scatterer and λ is the wavelength. An approach to solving this problem is known as NFFFT, in which the scattered field measured by a probe antenna on a scanning path in the near zone of the target is used in processing procedure to predict the scattered field in the far zone and, therefore, RCS of the target [1]. An attractive version of NFFFT, which is referred to as image based, builds a radar image of the scatterer and use it to calculate RCS [2]. Radar images provide important information about scattering properties of targets, and they are obtained in the framework of the image-based NFFFT at no extra cost. An overview of the practical implementation of the image-based NFFFT can be found in [3].

The scanning path can be chosen as a circle in space around the object (Fig. 1) if the size $D_\perp$ of the target in the direction perpendicular to the plane of the circle is such that the far-field criterion is satisfied at the position of the probe, i.e. $D_\perp < \sqrt{0.5\lambda\rho_0}$ where ρ_0 is the radius of the scanning circle. Several versions of such circular NFFFT are available in the literature [1-4]. To calculate the radar image from the input signal $U(k,\phi_0)$ in the monostatic case, a conventional image-based circular NFFFT uses the focusing operator

$$\psi(\rho,\phi) = \frac{e^{-2jk\rho_0}}{\pi^2\rho_0^2}\int_0^{\infty}\int_0^{2\pi} U(k,\phi_0)\left|\bar{\rho}-\bar{\rho}_0\right|^2 e^{2jk|\bar{\rho}-\bar{\rho}_0|}k\;dk\;d\phi_0 \tag{1}$$

with ρ and ϕ being the polar coordinates, $\left|\bar{\rho}-\bar{\rho}_0\right| = \left[\left(x-\rho_0\cos\phi_0\right)^2+\left(y-\rho_0\sin\phi_0\right)^2\right]^{1/2}$ and $k = 2\pi f/c$. To exclude the frequency dependence of the measurement facility, $U(k,\phi_0)$ can be conveniently defined as the ratio of the fields scattered from the target and from a calibration scatterer [4]. Once the radar image is available, the far-field backscattering cross section in the plane $z = 0$ (RCS in the waterline plane) is obtained as

$$\sigma(k,\phi) = \sigma_{\text{cal}}\left|\int_{-\infty}^{\infty}\int_{-\infty}^{\infty}\psi(x,y)e^{2jk(x\cos\phi+y\sin\phi)}dxdy\right|^2 \tag{2}$$

978-1-4244-6051-9/11/$26.00

where σ_{cal} is RCS of the calibration target. In [5] it has been shown that the use of focusing operator (1) may lead to significant errors in RCS for scanning paths of smaller radii or for scatterers with pronounced scattering centers offset from the geometrical center of the imaging area and the introduction of the factor

$$g(\bar{\rho},\bar{\rho}_0)=\frac{\rho_0^2}{\left|\bar{\rho}-\bar{\rho}_0\right|^2}\left[1-\frac{x}{\rho_0}\cos\phi_0-\frac{y}{\rho_0}\sin\phi_0\right] \tag{3}$$

under the integration sign in (1) can significantly improve the results. Figure 2 gives an example by presenting RCS of a single electrically small PEC sphere which is shifted from the center of the imaging area by 0.5 m and the scattered field is measured over a scanning circle of radius 1.5 m at the frequency 1 GHz. For this particular geometry, the conventional focusing operator results in an inaccurate curve (red) which strongly deviates from the exact black line. The correction factor $g(\bar{\rho},\bar{\rho}_0)$ from (3) significantly improves the agreement (blue curve).

One-dimensional scanning paths do not suffice if the size of the target in the direction perpendicular to the measurement plane is such that $D_\perp > \sqrt{0.5\lambda\rho_0}$. In this case, a scanning surface (e.g. spherical or cylindrical) enclosing the scatterer is necessary. In this paper we study the case of the cylindrical scanning surface and extend the two-dimensional approach presented in [5] to the three-dimensional case. The key point is the construction of a suitable focusing operator and similarly to the approach in [5], this is achieved by requiring that the radar image of an electrically small PEC sphere be given by the delta function. The presented version of NFFFT assumes a monostatic configuration with a point probing antenna but can be extended to bistatic configurations and probes with directivity patterns.

2. Processing Algorithm

The configuration under study consists of a cylindrical scanning surface of radius ρ_0 with $z_0^{\min}\le z_0\le z_0^{\max}$ and an imaging cylindrical region of radius $\rho_{\max}$ with $z_{\min}\le z\le z_{\max}$ (Fig. 1). A target is to be entirely located in the interior of the imaging region. A probing antenna moves over the scanning surface with the step $\delta\phi_0$ in the azimuth ϕ_0 and δz_0 in the vertical coordinate z_0, and at every point (ρ_0,ϕ_0,z_0) the scattered field is measured over a frequency range $f_{\min}\le f\le f_{\max}$ with a step δf . The input signal $U(k,\phi_0,z_0)$ is the ratio of the field $E^{\text{sc}}_{\text{tar}}(f,\phi_0,z_0)$ scattered by the target to the calibration field $E^{\text{sc}}_{\text{cal}}(f,\phi_0,0)$ scattered by a calibration target located at the center of the imaging area and measured in the plane $z_0=0$. In contrast to (1), the focusing operator should involve integration over z_0, and in order to determine the proper weighting function under the integration sign we require that the image of an electrically small PEC sphere of radius a_1 located at a point $\bar{r}_1$ be given by the delta function

$$\Psi(x,y,z)=V_1\delta(\bar{r}-\bar{r}_1) \tag{4}$$

where $V_1=4\pi a_1^3/3$ is the volume of the sphere. By direct substitution it can be shown that the focusing operator

$$\Psi(x,y,z)=\frac{4}{9\pi^{5/2}}\int_0^{\infty}dk\int_0^{2\pi}d\phi_0\int_{-\infty}^{\infty}dz_0\,\frac{A_{\text{cal}}(k)}{\left|\bar{r}-\bar{r}_0\right|}\left(1-\frac{x}{\rho_0}\cos\phi_0-\frac{y}{\rho_0}\sin\phi_0\right)U(k,\phi_0,z_0)\,e^{2jk(\left|\bar{r}-\bar{r}_0\right|-\rho_0)}\,, \tag{5}$$

where $\left|\bar{r}-\bar{r}_0\right|=\left[\left(x-\rho_0\cos\phi_0\right)^2+\left(y-\rho_0\sin\phi_0\right)^2+\left(z-z_0\right)^2\right]^{1/2}$ and $A_{\text{cal}}(k)$ is the scattering coefficient of the calibration scatterer, complies with (4) as $\bar{r}\to\bar{r}_1$, provided that the probing antenna is located in the far field of the calibration scatterer. RCS in the plane $z=0$ is calculated as

$$\sigma(k,\phi)=\frac{81k^4}{16\pi}\left|\iint_S\psi(x,y)e^{2jk(x\cos\phi+y\sin\phi)}dxdy\right|^2 \tag{6}$$

where the integration region *S* is a circular cross section of the imaging region with radius $\rho_{\max}$ and

$$\psi(x,y)=\int_{z_{\min}}^{z_{\max}}\Psi(x,y,z)\,dz \tag{7}$$

is the two-dimensional reflectivity map. NFFFT defined by (5) and (6) is applicable to arbitrary targets as an electrically small PEC sphere is a physical model of an elementary scatterer and every scatterer can be represented by a sum of elementary scatterers.

In practical applications, the input function $U(k,\phi_0,z_0)$ is available in a bounded domain ($k_{\min} \le k \le k_{\max}$, $0 \le \phi_0 < 2\pi$, $z_0^{\min} \le z_0 \le z_0^{\max}$) at a discrete set of values of (f,ϕ_0,z_0) and the integration in (5) is performed for a discrete set of points (x,y,z) from the image region ($x^2+y^2 \le \rho_{\max}^2$, $z_{\min} \le z \le z_{\max}$). A suitable numerical integration scheme for (5)-(7) is, therefore, necessary which should also ensure an acceptable compromise between the degree of discretization and the accuracy of RCS values.

3. Simulation Examples

To illustrate the applicability of the proposed NFFFT and study the role of the transformation parameters such as the sampling rates in the input data and in the image domain, it is convenient to use a scattering configuration consisting of two electrically small PEC spheres. The electrical size of the configuration is determined by the distance *D* between the spheres which can be chosen such that the probe is located in the near field. Since the multiple scattering between the spheres can be neglected, RCS of the configuration is easily available in an analytical form (see, e.g. [6]) and can be used to estimate the accuracy of NFFFT. The test cases presented here have been obtained in the frequency range $0.5\ \text{GHz} \le f \le 1.5\ \text{GHz}$ for the spheres of radii $a_1 = 0.005$ m and $a_2 = a_1/\sqrt[3]{2} \approx 0.004$ m separated by $D = 1$ m and located in the interior of the image domain: $\rho_{\max} = 1$ m, $-1\ \text{m} \le z \le 1$ m. The scanning surface defined by $\rho_0 = 1.5$ m and $-2\ \text{m} \le z_0 \le 2$ m is located in the near-field region of the configuration as $2D^2/\lambda \approx 6.7$ m. A PEC sphere of radius $a_{\text{cal}} = 0.01$ m with $A_{\text{cal}}(k) = 3\sqrt{\pi}a_{\text{cal}}^3 k^2$ has been used as the calibration scatterer. Figures 3 and 4 illustrate the effect of the sampling rates $\delta\phi_0$ and δf on the quality of the radar image for the two spheres located at $x = 0$, $y = \pm 0.5$ m, $z = 0$ while $\delta z_0 = 0.25$ m and $\delta l = \delta x = \delta y = \delta z = 0.025$ m. It is seen that $\delta\phi_0$ and δf are related to the intensity of spurious contributions in the XY-plane. The smaller the sampling rates, the better images and, therefore, the better RCS curves are obtained. The image quality in the planes that include the OZ-axis is controlled by δz_0.

RCS of two configurations at $f = 1$ GHz with the spheres at $x = 0$, $y = \pm 0.5$ m, $z = 0$ (as in Figs. 3 and 4) and at $x = 0$, $y = 0$, $z = \pm 0.5$ m are shown in Figs. 5 and 6, respectively. The different orientation of the spheres with respect to the plane $z = 0$ dramatically changes the dependence of RCS on ϕ. The sampling rates in the input signal are fixed ($\delta f = 50$ MHz, $\delta\phi_0 = 3°$, $\delta z_0 = 0.25$ m), whereas the sampling rate δl in the image domain takes three different values: 0.1 m, 0.05 m and 0.025 m. With $\delta l = 0.025$ m ($\delta l < \lambda/10$), a good agreement between the exact and NFFFT curves is observed. The agreement can be further improved by refining the sampling rates, which, however, increases the calculation time.

5. References

1. I. J. LaHaie, "Overview of an Image-Based Technique for Predicting Far-Field Radar Cross Section from Near-Field Measurements," *IEEE Antennas and Propagation Magazine,* **45**, December 2003, pp. 159-169.

2. A. Broquetas, J. Palau, L. Jofre and A. Cardama, "Spherical Wave Near-Field Imaging and Radar Cross Section Measurement," *IEEE Transactions on Antennas and Propagation,* **46**, May 1998, pp. 730-735.

3. T. Vaupel and T. F. Eibert, "Comparison and Application of Near-Field ISAR Imaging Techniques for Far-Field Radar Cross Section Determination," *IEEE Transactions on Antennas and Propagation,* **54**, January 2006, pp. 144-151.

4. K. J. Nicholson and C. H. Wang, "Improved Near-field Radar Cross Section Measurement Technique," *IEEE Antennas and Wireless Propagation Letters,* **8**, 2009, pp. 1103-1106.

5. H. Kobayashi, A. Osipov and H. Suzuki, "An Improved Image-Based Near-Field-to-Far-Field Transformation," *Asia-Pacific Microwave Conference Proceedings*, Yokohama, Japan, 2010, 4 p.

6. G. T. Ruck, D. E. Barrick, W. D. Stuart and C. K. Krichbaum, *Radar Cross Section Handbook*, Plenum, 1970, sec. 3.

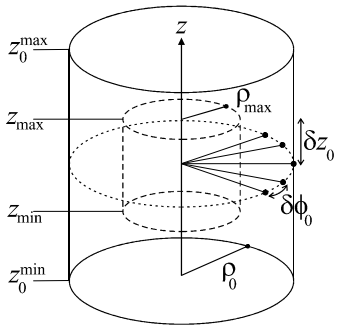

Fig. 1. A probing antenna moves over a cylindrical surface ($\rho_0 = \text{const}$, $0 \le \phi_0 < 2\pi$, $z_0^{\min} \le z_0 \le z_0^{\max}$) with steps $\delta\phi_0$ and δz_0 ; the target is placed inside the imaging region ($0 \le \rho \le \rho_{\max}$, $0 \le \phi < 2\pi$, $z_{\min} \le z \le z_{\max}$).

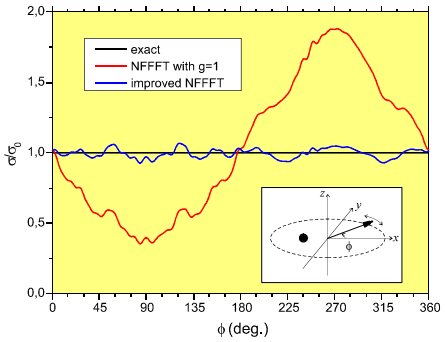

Fig. 2. RCS of a small PEC sphere offset from the center of the imaging area obtained with a conventional NFFFT (red) and with an improved version from [5] (blue); σ_0 is the theoretical RCS of the small sphere.

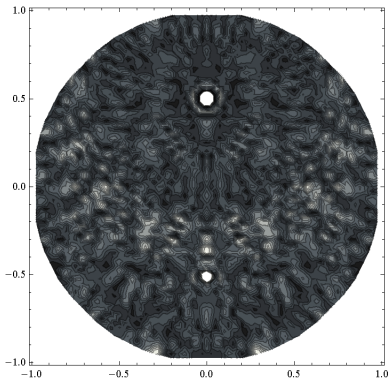

Fig. 3. Reflectivity map of two spheres in the plane $z = 0$ obtained with $\delta f = 200$ MHz and $\delta\phi_0 = 18°$; values of $|\psi(x, y)|$ are truncated at the level of 35% of their maximum to make spurious contributions visible.

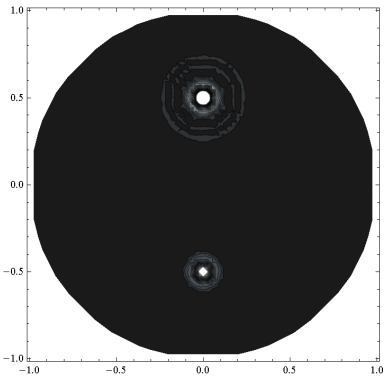

Fig. 4. The same as in Fig. 3, but with a finer discretization: $\delta f = 50$ MHz and $\delta\phi_0 = 3°$.

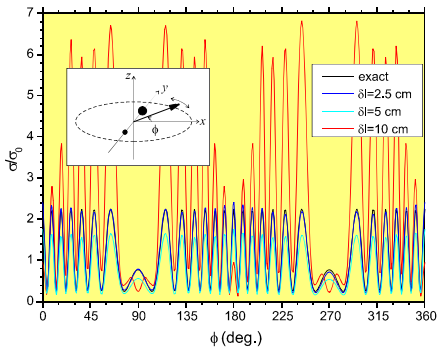

Fig. 5. RCS of two spheres located in the plane $z = 0$ at $f = 1$ GHz: exact result vs. NFFFT with different sampling rates δl .

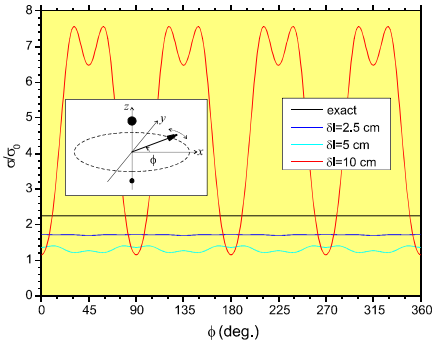

Fig. 6. The same as in Fig. 5, but with the spheres at the z axis.